Hindawi
Advances in Civil Engineering
Volume 2018, Article ID 1838370, 10 pages
https://doi.org/10.1155/2018/1838370

Research Article

Numerical Study of the Dynamic Compaction Process considering the Phenomenon of Particle Breakage

Xi Li,[1,2] **Jing Li**,[1] **Xinyan Ma**,[3] **Jidong Teng**,[1,4] **and Sheng Zhang**[1,4]

[1]*School of Civil Engineering, Central South University, Changsha, Hunan 410075, China*
[2]*School of Traffic and Transportation Engineering, Changsha University of Science and Technology, Changsha 410114, China*
[3]*China Airport Construction Group Corporation, Beijing 100101, China*
[4]*National Engineering Laboratory for High Speed Railway Construction, Changsha 410075, China*

Correspondence should be addressed to Xi Li; csu_lixi@csu.edu.cn and Sheng Zhang; zhang-sheng@csu.edu.cn

Received 16 June 2018; Revised 12 September 2018; Accepted 24 September 2018; Published 23 December 2018

Academic Editor: Annan Zhou

Dynamic compaction (DC) is commonly used to strengthen the coarse grained soil foundation, where particle breakage of coarse soils is unavoidable under high-energy impacts. In this paper, a novel method of modeling DC progress was developed, which can realize particle breakage by impact stress. A particle failure criterion of critical stress is first employed. The "population balance" between particles before and after crushing is guaranteed by the overlapping method. The performance of the DC model is successfully validated against literature data. A series of DC tests were then carried out. The effect of particle breakage on key parameters of DC including crater depth and impact stress was discussed. Besides, it is observed that the relationship between breakage amount and tamping times can be expressed by a logarithmic curve. The present method will contribute to a better understanding of DC and benefit further research on the macro-micro mechanism of DC.

1. Introduction

Dynamic compaction (DC) refers to the ground improvement method in which a heavy weight is dropped onto the ground surface from a great height to increase the density of the underlying soils. The DC method has been found to be useful in improving the mechanical behavior of underlying soil layers, especially loose granular materials [1–4]. Recently, the DC method has been widely used in many engineering fields, such as airports, seaports, dams, and railways.

Many analytical or semianalytical studies have been carried out to predict the important parameters involved in real DC treatments, including the degree and depth of improvement [5–7], the dynamic stress distribution in depth [8–10], the crater depth [5, 11, 12], and the numerical simulation of DC [13–18].

Although the topic of DC has been widely researched in geomechanics, the performance design and the application of dynamic compaction are still largely empirical in nature. This may be due to the complexity of the soil itself and the substantial challenges associated with a DC field test. Under the impact stress of a hammer, the soil foundation generates a series of complex responses, including the reorganization of local soil particles, the dramatic plastic deformation near the impact location, and the interior deformation under a stress wave. It is difficult to address all these responses in a deterministic model and collect sufficient data resources in a DC field test.

A numerical method simulation of DC attracts more attention in published literature. Poran and Rodriguez [13] presented one of the earliest 2D models for simulating DC in dry sand using the finite element code. Their computed results are good when the sand is relatively loose, but when densification occurs, the computed results depart substantially from experimental data. Based on the findings of Poran and Rodriguez, Lee et al. [14] and Gu et al. [15] described dry sand behavior under the DC process, utilizing

a finite element program. They discussed the effects of drop energy, the momentum of the falling tamper, and the tamper radius on the depth of improvement. In addition, they proposed a method for estimating the depth and the degree of improvement. Wang et al. [16] developed a method for estimating ground deformation with a numerical model created in LS-DYNA.

Considering numerical studies of DC, the discrete element method, which is neither limited by the large deformation nor the constitutive model of the soil, is superior [17, 18]. Ma et al. [18] pointed out that the improvement and the maximum influence depth of DC can be easily evaluated via the porosity changes of the gravel soil obtained by the particle flow discrete (PFC) element method. Jiang et al. [3] conducted a series of DC tests with PFC^{3D} to evaluate the compacting effects via the porosity and the ground settlement.

It is worth noting that particle breakage is unavoidable in the DC procedure and is more prone to occur for coarsely granular soil. Particle breakage will change the particle size distribution (PSD) and influence the soil mechanical properties. Previous literature has reported that particle breakage causes the PSD to behave as a soil variable, undermining the basic definition of soil and hence the soil mechanics principles [19–22]. However, the simulation of particle breakage is infrequently studied in the DC process. Further, little research has been carried out to study the effects of particle breakage on DC.

In this paper, a numerical study is carried out using the particle flow code in three dimensions (PFC^{3D}). Particular attention is paid to develop a numerical model of the DC process that can stimulate the phenomena of particle breakage caused by DC. The influence of particle breakage on crater depth and impact stress by DC is presented. The relationship between particle breakage amount and impact time is also discussed in detail.

2. Number Simulation of DC

2.1. Contact Model. The effect of dynamic hysteresis on the soil during DC is considered in this paper, and the hysteretic damping contact model is shown in Figure 1. The normal stiffness for loading, k_{n_load}, and unloading, k_{n_unload}, used in the hysteretic damping model is calculated by using the following equation:

$$k_{n\_load} = \frac{2R_h k_m}{1 + R_h},$$
$$k_{n\_unload} = \frac{2k_m}{1 + R_h}, \quad (1)$$

where the parameter R_h is the ratio of k_{n_load} to k_{n_unload} ($1.0 < R_h < 0.0$). The dynamic hysteresis of the soil is more apparent when the R_h is close to zero. The parameter k_m is the average normal stiffness of k_{n_load} and k_{n_unload}. The normal stiffness for unloading is greater than that for loading in the dynamic contact process, and a simple hysteresis loop is formed by the linear contact for particle loading and unloading.

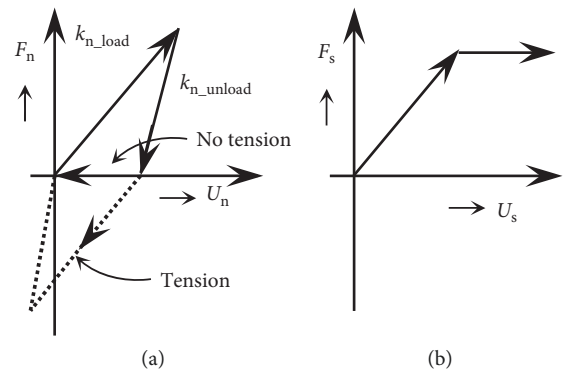

Figure 1: Constitutive relation of the hysteretic model: (a) normal direction; (b) shear direction.

2.2. Parameters of DC Model. The scale of the DC model and the calculation time cost are in conflict in PFC^{3D}. When preparing a numerical sample, the accuracy and the computing time needed in the DC model are taken into consideration. As shown in Figure 2, a cylindrical specimen with a height of 3.5 m and a bottom diameter of 3.5 m is used in this paper. Two walls, including one platen and a cylindrical wall, are created as the sample boundary. A total of 73318 balls, all with the same radius of 0.04 m, are created to stimulate the soil foundation. The hammer is simulated by 88 particles bound together by the "clump logic" code in PFC^{3D}. The diameter of the hammer is 0.5 m, the height is 0.2 m, and the weight of the hammer is 3 kN. The diameter of the hammer is 1/7 of the sample. The sample is large enough for the limited level of tamping energy.

To specify the values of microscale parameters in this DC model, the work from Wang et al., Ma et al., Wada et al., and Huang et al. [16–18, 23] is referenced, and the microscale parameters are determined, as shown in Table 1.

2.3. Simulation of Particle Breakage. The physical process of real particle breakage occurs when a single particle breaks into two or more smaller particles as the particle reaches a critical condition. Currently, particle breakage has been modeled by DEM with two alternative approaches.

The first approach is the fragment replacement method (FRM), in which single elements break and are replaced by a new generation of smaller grains, previously nonexistent in the simulation [24–27]. The second approach is the bonded-particle model (BPM), which indicates that a certain number of subparticles bond together to stimulate a single particle. The particle breaks if the magnitude of the force equals or exceeds the contact bond strength [28–31]. The first method repeatedly demonstrates superiority in computing time and particle breakage. Therefore, the FRM method is adopted in this paper.

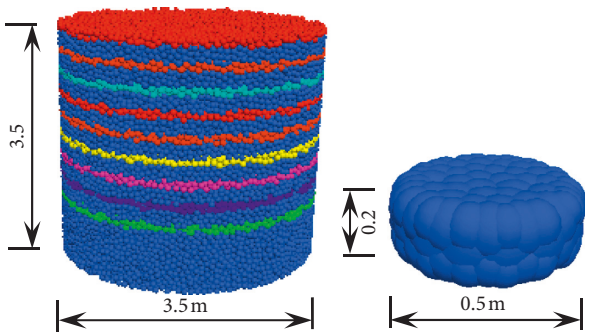

Figure 2: Discrete element model of dynamic compaction.

Table 1: Microscale parameters of PFC^{3D} model.

Parameters	Values
Particle number	73318
Particle density (kg·m^{-3})	2600
Particle radius (m)	0.04
Mass damping	0.70
Normal stiffness of the particles (N·m^{-2})	5×10^{6}
Tangential stiffness of the particles (N·m^{-2})	5×10^{6}
Hysteretic damping	0.50
Initial ground void ratio	0.40
Interparticle frictional coefficient	0.50
Tamp density (kg·m^{-3})	7800
Rammer gravity (N)	3000.30
Normal stiffness of the boundaries (N·m^{-2})	1.00×10^{8}
Tangential stiffness of the boundaries(N·m^{-2})	1.00×10^{8}
Poisson's ratio	0.30
m	10.00
d_0 (mm)	2.00
θ_0 (rad)	$\pi/18$
$\sigma_{lim,0}$ (Pa)	3.00×10^{9}

The two most important points in the FRM method are the particle failure criterion and the particle spawning procedure. The particle failure criterion is used to decide when a particle is crushed. The particle spawning procedure establishes the relationship between the disappearing broken particle and the new generation of smaller particles (subparticles).

2.3.1. Particle Failure Criterion. The particle failure criterion is a condition to determine when the particle breakages occur. Astrom and Herrmann [32] and Marketos and Bolton [33] adopted this condition directly as the maximum contact force acting on the particle. Lobo-guerrero [34] suggests the use of a limit tensile strength, which is related to forces acting on discs, similar to a Brazilian test. Ben-Nun and Einav [35] use explicit multiplicative correction factors to account for the effects of the coordination number and the contact curvature.

A multiaxial failure criterion was presented by Russell et al. [36] with the analysis of the elastic stress distribution induced by point loads on a sphere. An analytical expression for the maximum mobilized shear strength for a diametrically loaded sphere was obtained. The failure criterion for particle breakage can be expressed as

$$\kappa_{mob} \le \kappa, \tag{2}$$

where κ_{mob} and κ are the mobilized and intrinsic strengths of the grain, respectively. The value of κ is given by

$$\kappa = \frac{1+\chi}{\sqrt{3}}\left|\sigma_c\right|, \qquad \chi = \frac{\left|\sigma_c\right|}{\sigma_t} - 1, \tag{3}$$

where χ is a parameter of the microstructure properties of the materials. For most geological materials, χ ranges from 10 to 170. σ_c and σ_t are the uniaxial compressive strength and the tensile strength, respectively.

κ_{mob} is the maximum stress at the center of the contact area (Figure 3), and an approximate expression for the maximum mobilized strength valid for small contact angles is

$$\begin{aligned}\kappa_{mob} &= \frac{F}{\pi R^2 \sin^2\theta_0}\times\frac{\sqrt{3}\left(1+\chi^2\right)}{\chi} \\ &\quad\times\frac{((3/32)+(\sqrt{2}/24)+((\sqrt{2}/12)-(1/4))\nu+((1/2)-(\sqrt{2}/3))\nu^2)}{(2-\sqrt{2})(1+\nu)} \\ &= \frac{F}{\pi R^2\sin^2\theta_0} f(\chi,\nu),\end{aligned} \tag{4}$$

where ν is the Poisson's ratio, F is the load, R is the particle radius, and θ_0 is a solid angle "seen" from the center of the particle, defining the small area of stress application (Figure 3). Substituting Equation (4) into Equation (2) results in a limiting criterion for the normal contact forces as follows:

$$F_{lim} \le \frac{\kappa}{f(\chi,\nu)}\pi R^2\sin^2\theta_0 = \sigma_{lim}A_F. \tag{5}$$

As indicated in Equation (5), the limiting force F_{lim} is obtained from the limit strength σ_{lim} and a contact area A_F.

In this paper, the size effect is incorporated as a dependent of the mean strength value of the particle diameter through a correction factor f_{size}, which can be calculated in a Weibull form:

$$f_{size}(d) = \left(\frac{d}{d_0}\right)^{-3/m}, \tag{6}$$

where m is a material parameter, d is the particle diameter, and d_0 is the reference diameter (chosen as 2 mm). Then, the value of σ_{lim} can be expressed as

$$\sigma_{lim} = \sigma_{lim,0} f_{size}(d), \tag{7}$$

where $\sigma_{lim,0}$ is the mean limit strength at d_0.

To evaluate the contact area A_F in Equation (5), the Hertzian contact theory is adopted in this work. The radius of the contact area is determined by

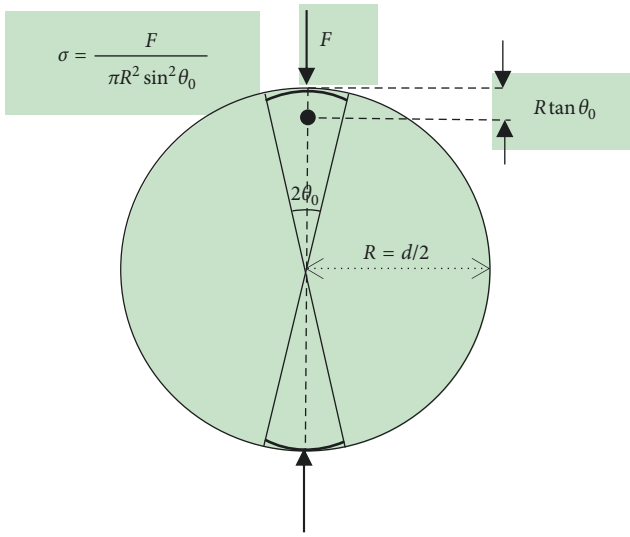

Figure 3: Force F acts normal to the sphere surface on an area defined by the angle θ_0.

$$r_F = \left(\frac{3Fr'}{4E'}\right)^{1/3},$$
$$r' = \left(\frac{1}{r_1} + \frac{1}{r_2}\right)^{-1}, \quad (8)$$
$$E' = \left(\frac{1-\nu_1^2}{E_1} + \frac{1-\nu_2^2}{E_2}\right)^{-1},$$

where r_1 and r_2 are the radiuses of the contacting spheres and E_1, ν_1, E_2, and ν_2 are their moduli. At this point, the criterion of particle breakage is developed.

2.3.2. Subparticle Substitution Model. For the method that replaces the broken parent particles with subparticles, we must ensure the mass conservation and reduce the local stress prominence caused by the overlap of the particles. This challenge needs to be considered because of the inevitable gaps between subparticles. The subparticle overlapping method is adopted in this paper. This method satisfies mass conservation by producing overlapping subparticles within the boundary of the original particle, and then, the subparticles are dispersed with an interaction force. McDowell and de Bono [24] pointed out that particle overlap causes the particle fragments to move as a single particle would when crushed between flat platens. To ensure sample stability and to accommodate the artificial pressure increase, in this study, particle breakages are updated immediately after the number of computational steps, equivalent to 0.003 s. This period is deemed sufficient to allow the artificially induced energy to dissipate.

As for the number of subparticles, Takei et al. [37] noted that the number of fragments after particle crushing is generally smaller than 10 for quarts particles. Research of McDowell and de Bono [24] shows that the number of subparticles has little or no effect on the one-dimensional normal compression lines. Therefore, four subparticles were chosen in this model. As shown in Figure 4, a particle will split into four equally sized smaller subparticles once the breakage criterion is satisfied. The subparticles inherit the velocity and material parameters of the mother particle at once. Mass conservation is strictly obeyed, and the particle breakage effect on the soil foundation is vastly minimized in the model.

2.4. Process of Dynamic Compaction. The DEM model of DC consists of two main processes, i.e., sample preparation and dynamic tamping. The specific steps of DC are as follows:

(1) A total of 73318 particles were created in the cylindrical space enclosed by the walls. The parameters of the particles are shown in Table 1. The particles were consolidated in the designated space under the influence of gravity (the acceleration of gravity was set to 9.8 m/s^2 in this study).

(2) The heavy hammer was created immediately above the center of the soil sample and free falling under the action of gravity. To improve the calculation efficiency, the drop height of the hammer was set by the initial velocity ($\sqrt{2gH}$) in this study.

(3) During each tamping process, key parameters such as displacement, velocity of the hammer, and contact stress between the hammer and foundation are monitored. The tamping process is complete when the hammer velocity decreases to 0 and the amount of crater depth no longer increases.

(4) The hammer is regenerated above the soil and assigned a specific initial speed for the next tamping. In this study, tamping with the same falling distances was carried out at the same point of the soil foundation, and the drop height of the hammer was 2 m, 4 m, 6 m, 8 m, and 10 m, respectively. For each height, the sample was tamped 10 times.

3. Verification of the DC Model

The particles of the gravel soil are treated as spheres in PFC^{3D}. In this paper, the applicability of the model is verified with the results from field tests.

Figure 5 shows the time-displacement curve of the hammer when the drop height is 2 m. Although the value of the crater depth from the DC model is not in total agreement with that of the field tests, the time-displacement curve obtained from this DC model shares the same characteristics with field tests [38, 39]. For a single DC process, the displacement of the hammer increases rapidly until the lowest point is reached and finally tends to be stable. For repeated DC, the crater depth first increases with the amount of compaction and then tends to be stable, which agrees with the physical process of the increase in the soil density and the modulus after DC.

Figure 6 shows the time-stress curve of the bottom of the hammer when the drop height is 2 m. It can be seen that the dynamic stress at the bottom of the hammer has a single

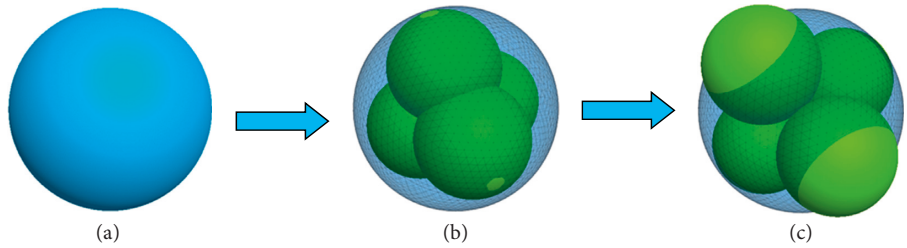

Figure 4: The configurations of postcrushing replacement.

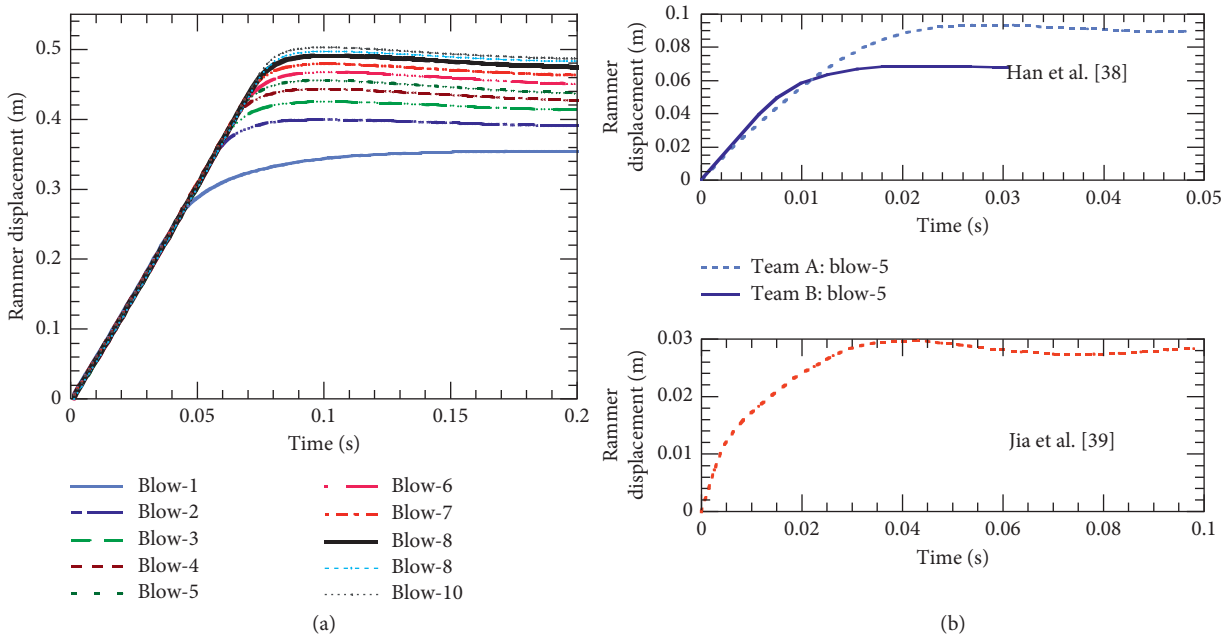

Figure 5: Hammer displacement over time in different studies: (a) displacement in this paper; (b) displacement in [38, 39].

peak triangle; the stress increment rate in the impact loading stage is obviously larger than the rate in the unloading stage. The results are also the same as those of Han et al. [38] and Jia et al. [39]. Therefore, it is inferred that the established DC model is sufficient to predict the whole tamping process.

4. Effect of Particle Breaking on DC

In DC practice, the crater depth of each impact is widely adopted to determine the optimal number of blows, and the impact stress is the direct indication of ground strength. The crater and the dynamic stress are two key parameters in the study of DC. Therefore, the effect of particle breakage on these two key parameters will be analyzed in this section.

4.1. Effect of Particle Breakage on Crater Depth. In the process of 10 blows, the depth of the crater per drop was analyzed with and without particle breakage. Figure 7 shows the crater depth under different drop heights. As shown in Figure 7, it is obvious that the crater depth increases with an increasing

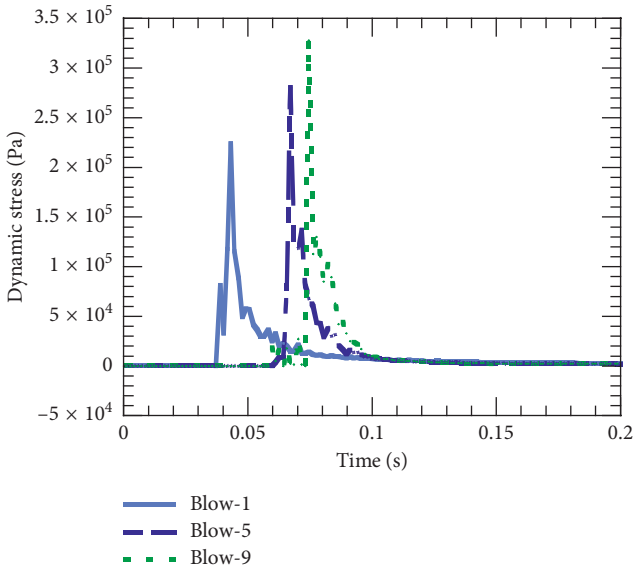

Figure 6: Time-stress curve of the bottom of the hammer.

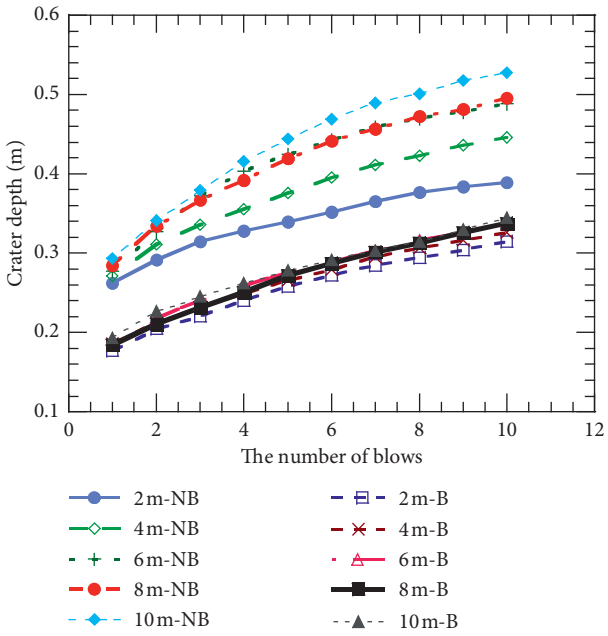

Figure 7: The crater depth under different dropping distances (NB means no particle breakage; B means particle breakage).

drop height for the same number of blows in both cases. Although the crater depth increases with an increasing number of blows, the amount of the increase decreases.

It is notable that the crater depth changes significantly with the occurrence of particle breakage during the DC process. Under the same DC conditions, particle breakage leads to a decrease in crater depth. For example, in the case of a 10 m drop height and 10 blows, the crater depths are 0.53 m without particle breakage and 0.34 m with particle breakage. The crater depth is reduced by 35.8%. In addition, particle breakage will decrease the crater difference caused by the drop height. The main reason for this decrease is that particle breakage consumes part of the tamping energy and the gap between the subparticles generated after particle breakage.

Particle breakage is only concentrated near the point of tamping. Hence, the effect of particle breakage on the increase in crater depth is limited. The true reason for tamping settlement is the accumulation of particle relative movement. All the microcosmic relative movements add up to a macroscopic tamping settlement. However, particle breakage requires tamping energy, and fewer particles are able to make the relative movement.

4.2. Effect of Particle Breakage on Dynamic Stress. To compare the effect of particle breakage on the dynamic stress in the DC process, 10 soil samples with same parameters were prepared. A series of DC tests were conducted with and without considering particle breakage at drop heights ranging from 2 m to 10 m. The results are shown in Figure 8.

As shown in Figure 8, particle breakage led to an increase in the peak value of impact stress, with the exception of the case of a drop height of 8 m. The dynamic stress of the bottom of the hammer without considering particle breakage at 2 m, 4 m, 6 m, and 10 m increased by 45%, 37%, 35%, and 47%, respectively, when compared to the dynamic stress if particle breakage was considered.

5. Particle Breakage during DC Process

In this section, the evolution of particle breakage during the DC process is analyzed. Considering that particle breakage occurs mostly near the compaction point, the change in particle size distribution (PSD) is investigated within a cylindrical area of diameter 0.7 m and height 0.5 m.

Figure 9 shows the evolution of PSDs with an increasing number of blows from a constant drop height of 10 m. It can be seen that the PSD curve lifts with an increase in the number of blows, indicating that the content of fine particles increases and the particle breakage aggravates.

By using the parameter of the breakage index proposed by Einav [40], the relationship between B_r and the number of blows from different drop heights is shown in Figure 10. It can be found that the larger the input energy (drop height) is, the larger the amount of breakage is. In addition, the breakage index increases with an increasing number of blows. However, the increment decreases with the number of blows. It appears that the relationship between B_r and the number of blows can be expressed by a logarithmic function.

6. Conclusions

Numerical simulations of the dynamic compaction process for gravel soil ground were developed in this paper via a particle flow code in three dimensions. The focus of the paper was the study of the effects of particle breakage on DC which has not been addressed in previous DC literature. The following conclusions could be drawn:

(1) The three-dimensional numerical model can simulate the phenomenon of particle breakage in the dynamic compaction process. Mass conservation during particle breakage simulation can be ensured.

(2) Under the same tamping energy level, particle breakage reduces the crater depth and weakens the difference of crater depth between different energy levels. This can be explained by crushing energy consumption and the enlargement of the space volume of the subparticles after crushing.

(3) Particle breakage increases the impact stress by approximately 35%–47%. However, the increased impact stress is mainly used for particle breakage instead of increasing the amount of crater depth.

(4) Particle breakage mainly concentrates at the impact point. There is no particle breakage at other locations and the boundaries of the soil. Therefore, the broken particles cannot play a role of accelerating the consolidation of the ground soil. In addition, the extent of particle breakage and the number of tamping blows show a strong logarithmic relationship.

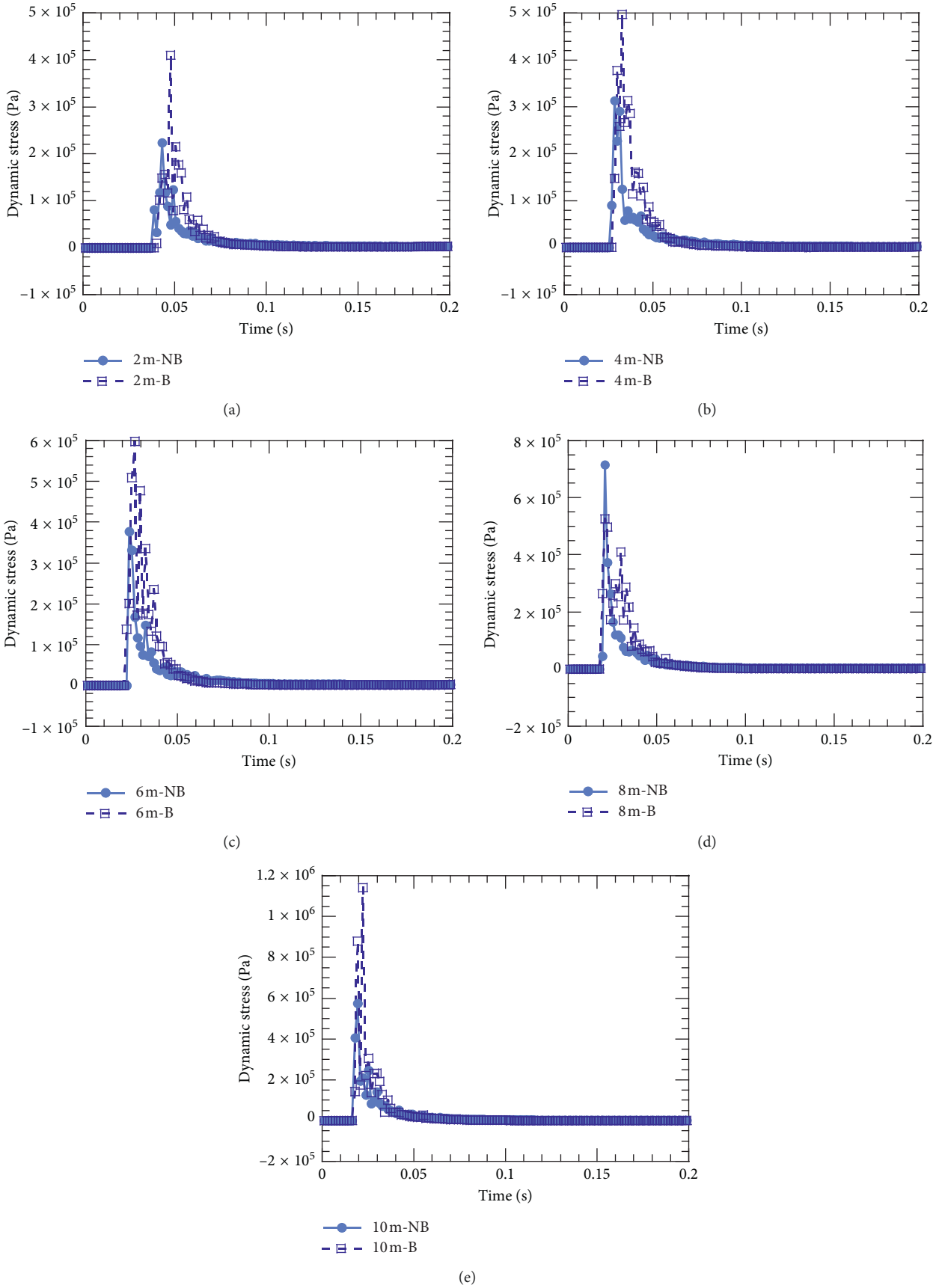

Figure 8: Time history of dynamic stress of tamper bottom (NB means no particle breakage; B means breakage).

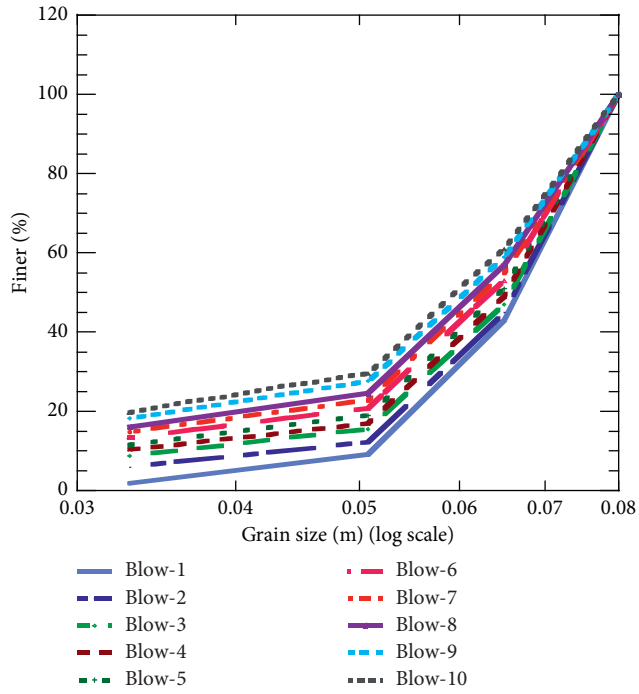

Figure 9: Particle gradation near the impact point under 10 blows.

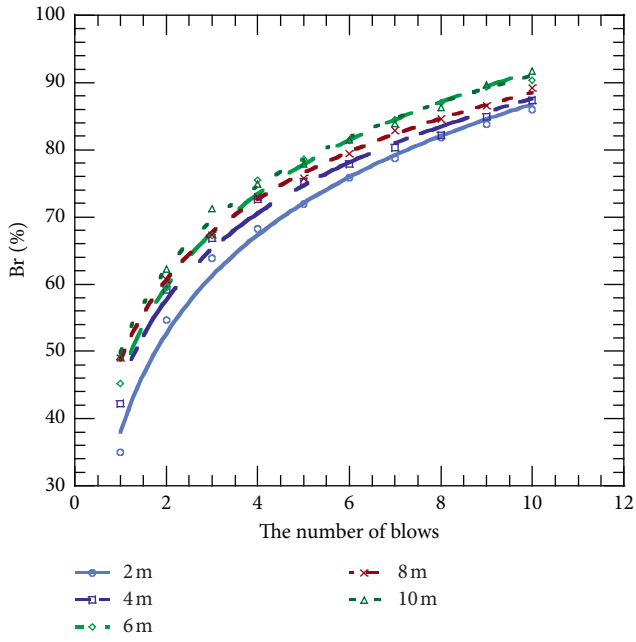

Falling distance (m)	$Br = a\ln(x) + b$		
x	a	b	r^2
2	21.23	37.9	0.990
4	18.60	44.7	0.989
6	19.83	45.8	0.996
8	17.33	48.6	0.999
10	17.91	49.82	0.996

Figure 10: The relationship between the relative breakage and the number of tamping blows.

(5) Soil behavior under the combined action of DC and particle breakage is a complex issue. This paper mainly focuses on the stimulation of the dynamic compaction process objectively. Other aspects that require further study include, but are not limited to, the optimal DC operational parameters, effective reinforcement depth, the assessment of the foundation strength, and the behaviors of particle breakage by dynamic compaction.

Data Availability

The data used to support the findings of this study are available from the corresponding author upon request.

Conflicts of Interest

The authors declare that they have no conflicts of interest.

Acknowledgments

This research was supported by the Natural Science Foundation of China (No. 51722812), Natural Science Foundation of Hunan Province (Grant No. 2017JJ1033), National Basic Research Program of China (No. 2014CB047001), and Central South University Autonomous Exploration Project (Grant No. 2017zzts150).

References

[1] P. W. Mayne, J. S. Jones, and J. C. Dumas, "Ground response to dynamic compaction," *Journal of Geotechnical Engineering*, vol. 110, no. 6, pp. 757–774, 1984.

[2] T.-W. Feng, K.-H. Chen, Y.-T. Su, and Y.-C. Shi, "Laboratory investigation of efficiency of conical-based pounders for dynamic compaction," *Géotechnique*, vol. 50, no. 6, pp. 667–674, 2000.

[3] M. Jiang, D. Wu, and B. Xi, "DEM simulation of dynamic compaction with different tamping energy and calibrated damping parameters," in *Proceedings of 7th International Conference on Discrete Element Methods*, pp. 845–851, Springer, Singapore, December 2017.

[4] Y. K. Chow, D. M. Yong, K. Y. Yong et al., "Dynamic compaction analysis," *Journal of Geotechnical Engineering*, vol. 118, no. 8, pp. 1141–1157, 1992.

[5] G. Mullins, M. Gunaratne, P. Stinnette et al., "Prediction of dynamic compaction pounder penetration," *Soils and Foundations*, vol. 40, no. 5, pp. 91–97, 2000.

[6] S. J. Feng, K. Tan, and W. H. Shui, "Dynamic compaction of ultra-high energy in combination with ground replacement in coastal reclamation areas," *Marine Georesources and Geotechnology*, vol. 33, no. 2, pp. 109–121, 2015.

[7] S. J. Feng, F. L. Du, Z. M. Shi et al., "Field study on the reinforcement of collapsible loess using dynamic compaction," *Engineering Geology*, vol. 185, pp. 105–115, 2015.

[8] P. W. Mayne and J. S. Jones, "Impact stresses during dynamic compaction," *Journal of Geotechnical Engineering*, vol. 109, no. 10, pp. 1342–1346, 1983.

[9] R. W. Pearce and R. A. Scott, "Soil compaction by impact," *Géotechnique*, vol. 25, pp. 19–30, 1975.

[10] R. L. Michalowski and S. S. Nadukuru, "Static fatigue, time effects, and delayed increase in penetration resistance after dynamic compaction of sands," *Journal of Geotechnical and Geoenvironmental Engineering*, vol. 138, no. 5, pp. 564–574, 2012.

[11] S. J. Feng, W. H. Shui, L. Y. Gao et al., "Field studies of the effectiveness of dynamic compaction in coastal reclamation areas," *Bulletin of Engineering Geology and the Environment*, vol. 69, no. 1, pp. 129–136, 2010.

[12] S. J. Feng, K. Tan, W. H. Shui, and Y. Zhang, "Densification of desert sands by high energy dynamic compaction," *Engineering Geology*, vol. 157, pp. 48–54, 2013.

[13] C. J. Poran and J. A. Rodriguez, "Finite element analysis of impact behavior of sand," *Journal of the Japanese Society of Soil Mechanics and Foundation Engineering*, vol. 32, no. 4, pp. 81–92, 2008.

[14] F. H. Lee and Q. Gu, "Method for estimating dynamic compaction effect on sand," *Journal of Geotechnical and Geoenvironmental Engineering*, vol. 130, no. 2, pp. 139–152, 2004.

[15] Q. Gu and F. H. Lee, "Ground response to dynamic compaction of dry sand," *Géotechnique*, vol. 52, no. 7, pp. 481–493, 2002.

[16] W. Wang, J. J. Chen, and J. H. Wang, "Estimation method for ground deformation of granular soils caused by dynamic compaction," *Soil Dynamics and Earthquake Engineering*, vol. 92, pp. 266–278, 2017.

[17] K. Wada, H. Senshu, and T. Matsui, "Numerical simulation of impact cratering on granular material," *Icarus*, vol. 180, no. 2, pp. 528–545, 2006.

[18] Z. Y. Ma, F. N. Dang, and H. J. Liao, "Numerical study of the dynamic compaction of gravel soil ground using the discrete element method," *Granular Matter*, vol. 16, no. 6, pp. 881–889, 2014.

[19] S. Zhang, C. X. Tong, X. Li et al., "A new method for studying the evolution of particle breakage," *Géotechnique*, vol. 65, no. 11, pp. 911–922, 2015.

[20] S. Zhang, X. Li, J. Teng et al., "A theoretical method for determining sample mass in a sieving test," *Computers and Geotechnics*, vol. 91, pp. 12–16, 2017.

[21] Y. P. Yao, W. Hou, and A. N. Zhou, "UH model: three-dimensional unified hardening model for overconsolidated clays," *Geotechnique*, vol. 59, no. 5, pp. 451–469, 2009.

[22] A. N. Zhou, D. Sheng, S. W. Sloan et al., "Interpretation of unsaturated soil behaviour in the stress – saturation space, I: volume change and water retention behaviour," *Computers and Geotechnics*, vol. 43, pp. 178–187, 2012.

[23] J. Huang, S. Xu, and S. Hu, "The role of contact friction in the dynamic breakage behavior of granular materials," *Granular Matter*, vol. 17, no. 1, pp. 111–120, 2015.

[24] G. R. McDowell and J. P. De Bono, "On the micro mechanics of one-dimensional normal compression," *Géotechnique*, vol. 63, no. 11, pp. 895–908, 2013.

[25] W. Zhou, L. Yang, G. Ma et al., "DEM analysis of the size effects on the behavior of crushable granular materials," *Granular Matter*, vol. 18, no. 3, pp. 1–11, 2016.

[26] M. B. Cil and G. Buscarnera, "DEM assessment of scaling laws capturing the grain size dependence of yielding in granular soils," *Granular Matter*, vol. 18, no. 3, pp. 1–15, 2016.

[27] M. O. Ciantia, M. Arroyo, F. Calvetti, and A. Gens, "An approach to enhance efficiency of DEM modelling of soils with crushable grains," *Géotechnique*, vol. 65, no. 2, pp. 91–110, 2015.

[28] M. B. Cil and K. A. Alshibli, "3D evolution of sand fracture under 1D compression," *Géotechnique*, vol. 64, no. 5, pp. 351–364, 2014.

[29] M. D. Bolton, Y. Nakata, and Y. P. Cheng, "Micro-and macro-mechanical behavior of DEM crushable materials," *Géotechnique*, vol. 58, no. 6, pp. 471–480, 2008.

[30] G. R. Mcdowell and O. Harireche, "Discrete element modelling of yielding and normal compression of sand," *Géotechnique*, vol. 52, no. 4, pp. 299–304, 2002.

[31] K. F. Zhang, S. Zhang, and J. D. Teng, "Influences of self-organization of granular materials on particle crushing based on discrete element method," *Chinese Journal of Geotechnical Engineering*, vol. 40, pp. 743–751, 2018, (in Chinese).

[32] J. A. Astrom and H. J. Herrmann, "Fragmentation of grains in a two-dimensional packing," *European Physical Journal B-Condensed Matter and Complex Systems*, vol. 5, no. 3, pp. 551–554, 1998.

[33] G. Marketos and M. D. Bolton, "Compaction bands simulated in discrete element models," *Journal of Structural Geology*, vol. 31, no. 5, pp. 479–490, 2009.

[34] S. Lobo-guerrero, "Crushing a weak granular material: experimental numerical analyses," *Géotechnique*, vol. 55, no. 3, pp. 245–249, 2005.

[35] O. Ben-Nun and I. Einav, "A refined DEM study of grain size reduction in uniaxial compression," in *Proceedings of the 12th international conference of the international association for computer methods and advances in geomechanics (IACMAG)*, pp. 702–708, Goa, India, October 2008.

[36] A. R. Russell, D. M. Wood, and M. Kikumoto, "Crushing of particles in idealised granular assemblies," *Journal of the Mechanics and Physics of Solids*, vol. 57, no. 8, pp. 1293–1313, 2009.

[37] M. Takei, O. Kusakabe, and T. Hayashi, "Time-dependent behavior of crushable materials in one-dimensional compression tests," *Soils and foundations*, vol. 41, no. 1, pp. 97–121, 2001.

[38] Y. H. Han, Y. L. Dong, and X. H. Bai, "Model test on process of hammer under dynamic compaction of loess," *Chinese Journal of Rock Mechanics and Engineering*, vol. 34, pp. 631–638, 2015, (in Chinese).

[39] M. C. Jia, L. Wang, and J. Zhou, "Mesomechanical analysis of characteristics of dry sands in response to dynamic compaction with PFC2D," *Rock and Soil Mechanics*, vol. 30, pp. 871–878, 2009, (in Chinese).

[40] I. Einav, "Breakage mechanics. part I. Theory," *Journal of the Mechanics and Physics of Solids*, vol. 55, no. 6, pp. 1274–1297, 2007.